

Validation of the MODIS LAI Product in Coniferous Forest of Ruokolahti, Finland

Yujie Wang^a, Curtis E. Woodcock^a, Wolfgang Buermann^a, Pauline Stenberg^b, Pekka Voipio^c,
Heikki Smolander^c, Tuomas Häme^d, Yuhong Tian^a, Jiannan Hu^a,
Yuri Knyazikhin^a, Ranga B. Myneni^a

^a*Department of Geography, Boston University, Boston, MA 02215, USA*

^b*Department of Forest Ecology, University of Helsinki, FIN-00014, Finland*

^c*Finnish Forest Research Institute, Suonenjoki Research Station,
FIN-77600 Suonenjoki, Finland*

^d*VTT Automation, Remote Sensing Group, FIN-02044 VTT, Finland*

Correspondence

Yujie Wang

University of Maryland, Baltimore County

Goddard Earth Sciences and Technology Center

1450 South Rolling Rd. Rm 3.002, Baltimore, MD, 21227, USA

email: yujie@umbc.edu

Telephone: 410-455-8807

Fax: 410-455-8806

Submitted for publication in

Remote Sensing of Environment

Abstract: Leaf area index collected in a needle-leaf forest site near Ruokolahti, Finland, during a field campaign in June 14-21, 2000, was used to validate Moderate Resolution Imaging Spectroradiometer (MODIS) LAI and FPAR algorithm. The field LAI data was first related to 30m resolution Enhanced Thermal Mapper Plus (ETM+) images using empirical methods to create a high resolution LAI map. It shows that comparisons at patch level are more reliable than the pixel level. Comparison of the aggregated high resolution LAI map and corresponding MODIS LAI retrievals imbues confidence in the MODIS LAI and FPAR algorithm. However, the MODIS algorithm, adjusted to high resolution, generally overestimates the LAI due to the influence of the understory vegetation, indicates the need for improvements in the algorithm. An improved correlation between field measurements and the Reduced Simple Ratio (RSR) suggests that the shortwave infrared (SWIR) band may provide valuable information for needle-leaf forests.

1 Introduction

Leaf area index (LAI) is a critical variable for understanding the biological and physical processes associated with vegetated land surfaces, and thus is a key input of climate and large-scale ecosystem models (Foley et al., 1998; Sellers et. al, 1997; Bonan, 1996; Dickinson et. al., 1986). LAI is defined as one-sided green leaf area per unit ground area in broadleaf canopies and as the hemisurface needle leaf area in coniferous canopies (Chen et. al., 1992; Stenberg, 1996; Knyazikhin et. al., 1998a). For effective use in global-scale models, this variable must be collected over a long period of time and should represent every region of the terrestrial surface. LAI is operationally produced from MODERate Resolution Imaging Spectroradiometer (MODIS) data. The Terra platform, with MODIS and other instruments, was launched in December 1999 and data collection began in March 2000. The LAI and FPAR products are at 1 km resolution at an 8 day interval. The product was made public in August 2000 through the EROS (Earth Resources Observation System) Data Center Distributed Active Archive Center. Presently, the emphasis within the MODIS program is on validation of the algorithm and its products (Privette et. al., 2002).

Global validation of moderate to coarse resolution LAI products is a complicated and challenging task. It involves field measurements at sites representative of a wide range of vegetation types and scaling of field measurements from small areas to the resolution of satellite data. Also, one should account for uncertainties in inputs to the retrieval techniques due to uncertainties in registration, correction for atmosphere effects, etc, which make the comparison of ground-based measurements with coarse resolution data a complicated task. The development of appropriate ground-based sampling strategies is critical to an accurate specification of uncertainties in the LAI product (Tian et. al., 2002b).

In this study, we will evaluate the MODIS LAI product which includes (a) creation of a 30m resolution LAI map using data from a field campaign in Ruokolahti, Finland, and 30 m Landsat Enhanced Thermal Mapper Plus (ETM+) images, and (b) comparison of the MODIS LAI map with the fine resolution LAI map aggregated to the MODIS resolution.

2 Experiment Descriptions

2.1 Validation Site and Sampling Strategy

A 1x1 km area of needle leaf forest near Ruokolahti, Finland (61.32°N, 28.43°E), was chosen for field data collection to validate the MODIS LAI/FPAR product. The site is mostly occupied by Scots pine (*Pinus sylvestris*) and Norway spruce (*Pices abies*), with pines dominant. The Ruokolahti Forest site is a typical northern needle leaf forest, mixed with large and small lakes. The height of the trees was between 5-20 meters. However, there was a small open area in this 1x1 km site, which was occupied by a mixture of re-growing smaller (less than 1.5 m in height) pine trees, dwarf shrubs and an understory of grasses. The 1x1 km site was divided into 20 rows and 20 columns, for a total 400 grid points. Each point was 50 meters apart. Additionally, the canopy was stratified into young, intermediate and dense needle forests based on examination of an airborne 2-meter resolution Charge-Couple Device (CCD) image. The young forest is represented by the area mentioned above with small trees and understory grasses. Within each class, data at a higher resolution, 25m, in subplots of 100×150 m and 200×200 m were also collected (Figure 1). The LAI of the young forest understory was not measured during this field campaign.

2.2 Instrumentation and Data Collection

Leaf area index (LAI), canopy and ground spectral reflectances were measured at this site during June 14th to 21st of 2000. LAI was measured with a LAI-2000 plant canopy analyzer (Li-

Cor, Inc., Lincoln, Nebraska), which consists of a LAI-2070 control unit and a LAI-2050 sensor head. The sensor head projects the image of its nearly hemispheric view onto five detectors arranged in concentric rings (approximately 0-13, 16-28, 32-43, 47-58, 61-74 degrees). A 270 degree view cap was used to eliminate the operator's shadow. Two LAI-2000 units were used to take simultaneous measurements within the forest and in an open area. They were inter-calibrated. The measurements were taken shortly before sunset, or during overcast days, when the forest was illuminated only by diffuse light. We followed the calibration procedure given in the LAI-2000 Plant Canopy Analyzer Instruction Manual, chapter 4-1 (LI-COR, 1992).

LAI values were calculated according to Miller's derivation (Miller, 1967), which is the default method used by LAI-2000. It should be noted, however, that the LAI-2000 converts canopy gap fraction into LAI under the assumption of uniformly distributed leaves (needles) and, moreover, the instrument cannot distinguish between foliage and woody material. Values from the Miller's formulae, therefore, give an effective leaf area index, L_e , which can be converted to the LAI as (Chen and Cihlar, 1996)

$$\text{LAI} = (1 - \alpha)L_e\gamma_e / \Omega_e , \quad (1)$$

where α is the woody-to-total area ratio, γ_e is the needle-to-shoot area ratio, and Ω_e is the element clumping index. In the MODIS LAI/FPAR algorithm, a one-year old shoot is taken as the basic foliage element (Knyazikhin et. al., 1997; Tian et. al., 2002; Wang et. al., 2002), uniformly distributed within the tree crown, and its projected silhouette area is taken as the foliage area, i.e., MODIS provides LAI values corresponding to equation (1) with $\gamma_e = 1$ and $\Omega_e = 1$. Values of the woody-to-total area ratio were set to 0.16. This value was obtained by averaging all values of α corresponding to needle forest sites reported by Chen and Cihlar (1996), as the required data for our site were not available.

GPS locations were made and differential correction performed within each grid level of the 1x1 km plot. Thus, a set of accurate geolocation measurements, with an uncertainty of about 2 m was obtained.

An ETM+ image collected on June 10, 2000 was used to generate a fine resolution LAI map in our study. The image was atmospherically corrected using a simplified method for atmospheric correction (SMAC) algorithm (Häme et. al., 2001; Rahman & Dedieu, 1994). The ETM+ image was coregistered to the CCD image.

3. Data Analysis

Figure 2 presents histograms of ETM+ red and near-infrared (NIR) reflectances of young, intermediate and dense forests sites. Table 1 shows the mean values of these histograms and their standard deviations. The young forest has distinct reflectance features compared to the others. The distributions of the ETM+ reflectances of the intermediate and dense forests are almost indistinguishable in these spectral bands. Typically, the reflectances of the intermediate and dense forests are about 0.023 in the red, and about 0.20 in the NIR bands. For the young forest, reflectances in these spectral bands are 0.07 and 0.27, respectively.

Figure 3 presents histograms of effective LAI values for young, intermediate and dense forests collected at spacings of 25 m and 50 m in the same subplots. Table 2 shows mean values of these histograms and their standard deviations. The mean effective LAI for the dense and intermediate forests are almost unchanged with sampling frequency. However, for the young forest, because the measuring height varied between the two measurements (25m spacing measurement was performed at ground level while 50m spacing measurement was performed at 1 m height), the mean values are substantially different. The t-test results show that the mean effective LAI values are not significantly different in the case of the dense and intermediate

forests, while mean values for the young forest are not statistically equal (Table 2). Table 2 also shows that, generally, dense sampling results in lower variance, as would be expected.

In the three subplots, some grid points were measured twice because the subplots overlapped with the 50 m grid. These measurements were used to assess the uncertainty in the LAI measurements. Figure 4 shows the correlation between LAI measured at 50 m grid and corresponding 25 m subgrid. The R^2 is 0.93 and RMSE is 0.23. This RMSE value indicates the uncertainty in the LAI measurements. It also sets a limit to the accuracy of LAI maps derived from these field measurements.

A contour plot of the effective LAIs is shown in Figure 5a. One can see that the spatial distribution of the effective LAIs generally captures the spatial pattern of the 1x1 km site shown in the CCD picture (Figure 5b); that is, low LAI values within the open area and high LAI values near the lower-left and lower-right corners, where the dense canopies are located.

4. Derivation of a Fine Resolution LAI Map

The biggest challenge for validation of moderate (100-1000m) and coarse (> 1 km) resolution LAI products is the scarcity of ground-truth measurements. Considering the scale of *in situ* measurement (generally <10 m per sample) and the large amount of work associated with field measurements, it is unrealistic to expect sufficient data for a pixel-by-pixel comparison. An alternative is to employ both field measurements and high resolution satellite data to derive an accurate fine resolution LAI map over a sufficiently extended area, degrade it to the coarse resolution, and compare this map with that derived from the coarse resolution imagery. Thus, the first task is to derive a 30 m resolution LAI map of a 10 km by 10 km region centered on the site where LAI measurements were made.

4.1 Adjustment of MODIS LAI and FPAR Algorithm at 30 m Resolution

As a first attempt, the MODIS LAI and FPAR algorithm was adjusted to 30 m resolution to produce a 30 m resolution LAI map of the validation site using the ETM+ reflectances. The algorithm requires a 6-biome land cover classification (Myneni et. al., 1997). All ETM pixels were treated as needle forests except for the young forest class. This class was mostly occupied by understory grasses and small shrubs and hence was treated as grasses.

The MODIS LAI/FPAR algorithm uses a Look-Up Table (LUT) to retrieve LAI values. A three-dimensional radiative transfer equation is used to derive spectral and angular biome-specific reflectances of vegetation canopies. The numerical solutions of this equation are calculated and stored in the LUT. We begin with the Landsat TM LUT developed by Tian et. al. (2002c) for the Northwest US (Washington and Oregon). The resulting correlation between retrieved LAI and field measured LAI at the pixel scale is shown in Figure 6a. One can see that most of the retrieved LAIs are significantly greater than the field measured LAIs and their correlation is poor. Therefore, this LUT needed to be adjusted (Tian et. al, 2002a, 200b &2002c).

Three factors influence the LAI retrieval of the MODIS LAI/FPAR algorithm: a) background reflectance which is an averaged effective reflectance of the surface underneath the canopy (soil or/and understory canopy); b) canopy structure parameter which depends on the biome type and architecture of the vegetation canopy; c) single scattering albedo which is defined as the ratio of energy scattered by the elementary volume inside the canopy to the energy intercepted by this volume. In the LUT of the algorithm, global vegetation was classified into six biome types using a vegetation cover classification parameterized in terms of variables used by photon transport theory (Myneni et al., 1997), each representing a pattern of the architecture of an individual tree (leaf normal orientation, stem-trunk-branch area fractions, leaf and crown size) and the entire canopy (trunk distribution, topography), as well as patterns of spectral reflectance

and transmittance of vegetation elements. The soil and/or understory type are also characteristics of the biome, which can vary continuously within given biome-dependent ranges (Myneni et. al, 1999). The single scattering albedo describes the optical properties of elementary volume and varies significantly for different species in different parts in the world. A correct value of single scattering albedo is required to obtain reliable retrieval.

The single scattering albedo variable is assumed biome-specific constant with respect to spatial and directional variables in the algorithm. However it also depends on the definition of the scattering center and the size of elementary volume considered in the formulation of the radiative transfer equation. Since the canopy architecture also depends on the definition of the scattering center, the canopy structure parameter also depends on it. Therefore, the canopy structure parameter must be consistent with the single scattering albedo. For example, if a cube of 50x50x50 cm is taken as an elementary volume in a coniferous forest, a one-year shoot of 5-7 cm should be taken as a scattering center (Knyazikhin et. al., 1997). The single scattering albedo, in this case, characterizes scattering properties of the 50x50x50 cm cube filled with one-year shoots, and all coefficients of the transport equation should be derived for such 50x50x50 cells.

LAI is nonlinearly related to single scattering albedo and canopy structure parameter, nevertheless, changing the single scattering albedo will change the distribution of retrieved LAI. The LUT can be adjusted by tuning the single scattering albedo or canopy structure parameter to find the best match between algorithm retrieved LAI and field measured LAI. The LUT was adjusted through matching the distributions of retrieved LAI and field measured LAI. Figure 6b shows the results after tuning the single scattering albedo, which improves the overall relationship, but the results appear noisy. The reason for this is carefully analyzed in the following section.

4.2 Validation of MODIS LAI and FPAR Algorithm at 30 m Resolution

Although every effort has been made to obtain accurate geolocation of each sampling point and ETM+ pixels, this still does not guarantee that the sampling point falls within the specified satellite pixel. An illustration of pixel-by-pixel comparison is shown in Figure 7a. Field samples often fall on the boundary or out of the pixel. Moreover, one or even a few measurements in a single pixel may be insufficient to represent the pixel mean value because the area measured with the LAI-2000 is considerably smaller than ETM+ pixels. The LAI values in this forest area exhibit high variance over short distances, as first noted by Tian et. al (2002a). Based on a hierarchical decomposition of variograms (Woodcock et. al., 1997; Collins & Woodcock, 2000), Tian et. al. (2002b), proposed a patch based comparison method to scale field measurements to the spatial scale of satellite observations.

For the analysis of remotely sensed imagery, a landscape can be regarded as a collection of smaller objects, such as forests stands or other homogenous patches of vegetation. In essence, the landscape may be assumed to be composed of a set of objects which are more homogenous within than between them (Collins & Woodcock, 2000). In this situation, satellite pixels are assumed to be samples of objects. When pixels are small relative to objects, internal variance of the objects can adversely affect the analysis (Markham & Townshend, 1981). On the other hand, when the pixel size is large relative to the objects, an individual pixel often covers parts of two or more objects, resulting in mixed pixels, and the effectiveness of analysis is undermined (MacDonald & Hall, 1980). An ideal condition would result when remote measurements correspond directly to the objects in the scene (Woodcock & Harward, 1992), a situation which is not observed in nature due to the variance in object size.

One way to try to minimize the effects of sparse sampling of ETM+ pixels and possible geolocation errors, is to shift the scale of analysis from pixels to forest stands, or patches. The

patches should satisfy the following conditions: a) their internal variance is small such that a patch can be regarded as a relatively homogenous area and a small amount of sampling is sufficient to characterize the mean feature of the object; b) each patch should be large enough such that effect of geolocation errors is minimized. In this case, each point measurement can be regarded as a random sample of a larger area. This increases the probability that the sampling point falls inside the patch, with the mean value of these samples serving as an estimate of the true mean of the entire patch. Figure 7b shows the scheme of a patch-by-patch comparison. Without extraordinary registration accuracy and high sampling density, a patch-by-patch comparison is more reliable than a pixel-by-pixel comparison.

Image segmentation can be used to generate patches in images. The objective of image segmentation is to partition the image into a set of patches, which correspond to objects on the ground (Beaulieu & Goldberg, 1989). It groups pixels into patches based on their spectral similarity and adjacency. The decision of the size and number of patches are based on following considerations: a) patches can not be too small, which ensures enough field samples in each patch and reduce geolocation errors; b) patches can not be too big, which ensures enough number of patches for statistics and also preserves patch homogeneity. Using this method, the 1 km ETM+ image of the validation site was divided into 19 patches. Each consists of tens to hundreds of pixels and is relatively homogenous (Figure 8). Table 3 shows the mean values of red and NIR reflectances over these segments and their standard deviations. The coefficient of variation does not exceed 10^{-2} indicating that the segments can be treated as homogeneous areas with respect to their red and NIR reflectances. However, the LAI values exhibit higher variation within the patches (Table 4). If the coefficient of variation is taken as a measure of uncertainty, most of the patches can be represented by the mean LAI value within an uncertainty of 20%. However, in some segments (1,4,8 and 9) the uncertainty can be high.

The patch map shown in Figure 8 was then used to produce mean LAIs over each patch. Figure 9 demonstrates a patch-by-patch correlation between measured and retrieved LAI values. Although the correlation between retrieved LAI and field measured LAI is improved after adjustment of the LUT, significant disagreement still exists. The disagreement between the measured and retrieved LAI values is a decreasing function of LAI. One possibility is the effect of understory vegetation, as the field measurements do not capture the effect of the understory. Thus the field measurements only characterize the forest canopy yet the reflectance in the imagery includes the understory, which includes mosses, shrubs and small trees. In this situation, one would expect estimates of LAI from imagery to exceed those measured on the ground and the effect to be larger at low canopy LAI values as the understory is more visible from above, as is observed in Fig. 9b.

4.3 Generating a Fine Resolution LAI Map of the 1x1 km Using Empirical Approaches

In hopes of producing a better high resolution LAI map for comparison with MODIS retrievals, empirical methods were tested. Numerous similar studies have been performed to relate ground-measured LAI to satellite observations (Franklin, 1986; Spanner et. al., 1990; Nemani et. al., 1993; Chen & Cihlar, 1996; Fassnacht et. al., 1997; Tian et. al., 2002a&2002b). A widely used approach is to regress ground-measured LAI on vegetation indices such as the normalized differential vegetation index (NDVI) and the simple ratio (SR). The NDVI is the most commonly used vegetation index for LAI retrievals. This variable is defined in terms of red and NIR reflectances, ρ_{red} and ρ_{NIR} ,

$$NDVI = \frac{\rho_{NIR} - \rho_{red}}{\rho_{NIR} + \rho_{red}} \quad (2)$$

Figure 10a shows that the pixel-by-pixel correlation between field-measured LAI and satellite-derived NDVI is low; the R^2 is 0.23 in this case. These results appear noisy in much the same fashion as previous results based on pixels (Figure 6). As Tables 3 and 4 indicate, LAI values can vary considerably with reflectances in red and NIR spectral bands essentially unchanged. This results in poor correlation between the field measured LAI and satellite-derived NDVI.

The correlation improves considerably if patches are used as the element of the analysis. The correlation between mean NDVI and mean field-measured LAI of patches is shown in Figure 10b. The R^2 increases to 0.73 with a RMSE of 0.34. Note that mean reflectances of the patches were used in equation (2) to calculate the mean NDVI.

Although a good correlation can be obtained at the patch scale between NDVI and LAI, the dynamic range in NDVI is small. Figure 10b shows that mean NDVI values fall in the interval between 0.6 and 0.8, while the LAI values vary between 0.2 and 2.7.

The simple ratio (SR) is another index used to relate LAI values to satellite data. For a given area, this variable is the ratio of NIR to red reflectance. Figure 11 shows the pixel and patch level relationship between the SR and LAI. Again, the pixel level relationship is poor between field measured LAI and the SR ($R^2=0.20$). However, at the patch level, a better relationship is obtained ($R^2=0.82$, $RMSE=0.29$). The range of the SR is between 4.5 and 9.0. It should be noted that there is a direct but nonlinear relationship between the SR and NDVI; that is, $SR = (1+NDVI)/(1-NDVI)$, and thus SR and NDVI contain similar information.

The understory strongly affects the SR and NDVI. The influence of the understory on these variables can be quite high, as our field LAI measurements were taken for overstory canopy only. The understory NDVI can be as high as 0.6. The contribution of understory to NDVI or SR is also a function of canopy closure (Franklin, 1986; Spanner et. al., 1990). Several studies

suggest that the use of shortwave infrared (SWIR) reflectances can account for the background reflectances (Butera, 1986; Baret et. al., 1988; Nemani et. al., 1993; Brown et. al., 2000). A modified form of the simple ratio, or the reduced simple ratio (RSR) was proposed by Brown et. al. (2000):

$$RSR = \frac{\rho_{NIR}}{\rho_{red}} \left[1 - \frac{\rho_{SWIR} - \min(\rho_{SWIR})}{\max(\rho_{SWIR}) - \min(\rho_{SWIR})} \right] \quad (3)$$

where ρ_{SWIR} is the shortwave infrared reflectance, which can be obtained from Band 5 of ETM+ data, and the $\min(\rho_{SWIR})$ and $\max(\rho_{SWIR})$ are the minimum and maximum SWIR reflectance found in the ETM+ image. The advantages of RSR over SR are (Brown et. al., 2000; Chen et. al., 2002): a) the background influence is suppressed because the SWIR band is mainly sensitive to the amount of vegetation containing liquid water in the background; and b) the difference between cover types is reduced, so a single LAI algorithm can be developed without using a coregistered landcover map.

Figure 12 shows the relationship between RSR and LAI at the patch scale ($R^2=0.91$; $RMSE=0.22$). Note that the mean reflectance over the corresponding patch was used in equation (3) to calculate the patch RSR. The linear regression is

$$LAI = 0.4693RSR - 0.6277 \quad (4)$$

This relationship was applied to a 10 km by 10 km ETM+ scene centered on the validation site to generate a fine resolution LAI map. This 10 km area was first segmented into patches and then equation (4) was applied to each patch. Figure 13 shows LAI maps of the 10 km area and its central part, the 1km area, derived from the ETM+ image using the relationship (4). The LAI map of the 1x1km captures the basic spatial features shown in Figure 5b, namely, the young forest in the middle of the image, and the dense forest on the lower-left and lower-right corners.

The RMSE for the relationship (4) is 0.22 which is taken as a measure of the uncertainty. Assuming that relationship (4) is valid for the entire 10x10 km area, and assuming that uncertainties in the channel ETM+ data do not affect the reduced simple ratios (equation 3), one can conclude that the uncertainty of the fine resolution LAI map is 0.22. This is consistent with the estimation in figure 4 (RMSE=0.23).

5 Validation of the MODIS LAI Product

5.1 The MODIS LAI Product

The MODIS LAI and FPAR product is produced at 1 km spatial resolution daily (MOD15A1) and composited over an 8-day period based on the maximum FPAR value. The 8-day product (MOD15A2) is distributed to the public from the EROS Data Center Distributed Active Archive Center (EDC DAAC). The products are projected on the Integerized Sinusoidal (IS) 10-degree grid, where the globe is divided for production and distribution purposes into 36 tiles along the east-west axis, and 18 tiles along the north-south axis, each approximately 1200x1200km. Each tile contains LAI, FPAR and two quality assessment (QA) variable data sets (Myneni et al., 2002). The QA variable data sets contain information about retrieval status such as the overall quality of input data, cloud condition, algorithm used to retrieve LAI etc.

The MODIS LAI and FPAR algorithm uses a biome classification map and atmospherically corrected MODIS spectral reflectances at 1 km resolution to retrieve LAI and FPAR. It compares measured reflectances with those determined from a suite of canopy models, which depend on biome type, canopy structure, and soil/understory reflectances. The canopy/soil/understory models for which simulated and measured surface reflectances do not exceed uncertainties in model and observations are used to derive the distribution of all possible solutions, i.e., LAI and FPAR distribution functions. The mean values of these distribution functions are archived. The

overall uncertainty (Wang et al., 2001) in model and observations is set to 20%. This number is our best estimation of the overall uncertainty derived from SeaWiFS data (Kimes et. al., 2000; Knyazikhin et. al., 1998) and subject to change when uncertainty information about MODIS land surface reflectance is available. Should this main algorithm fail, a backup algorithm is triggered to estimate LAI and FPAR using vegetation indices. Information on which algorithm was used is archived in the QA variable data set. In the case of a dense canopy, its reflectance can be insensitive to various parameters (e.g., LAI) characterizing the canopy. When this happens, the canopy reflectance is said to belong to the saturation domain (Knyazikhin et al., 1998b). This situation is recognized by the retrieval technique (Knyazikhin et al., 1998b) and reported in the QA variables. It also should be noted that the MODIS algorithm is executed independently of information provided by the cloud mask. Therefore, users are required to consult the QA file to select LAI values retrieved under clear sky conditions.

5.2 Validation of the MODIS LAI Product

The 002 MOD15A2 product for days 169-177 (June 17-25, 2000) was used in our analysis. The Ruokolahti Forest is located in tile h19v02, line 1016 and sample 442. A region of 10x10 km centered on the validation site was extracted from the corresponding MODIS tile which was then coregistered to the ETM+ scene. LAI values produced by the main algorithm under clear sky conditions were selected. Figure 14 shows the distribution of selected pixels in the 10x10 km area which satisfy these criteria. Vegetated cloud free pixels for which the main algorithm was triggered made up 30% of all pixels. The 30 m resolution map derived using the regression based on RSR was aggregated to 1 km resolution by averaging all fine resolution LAI values within each MODIS pixel. LAI of water and barren pixels were set to zero. Figure 15 shows a contour plot of the aggregated LAI map. A pixel-by-pixel comparison between MODIS LAI and aggregated LAI is shown in Figure 16. Similar to the cases described earlier (Figs. 10a and 11a), MODIS LAI and aggregated LAI are poorly correlated ($R^2=0.33$) at the pixel scale.

Pixel-by-pixel comparison is not appropriate for the following reasons: a) the registration accuracy of a single pixel is not guaranteed, so the pixel aggregated from fine resolution may not match well with the MODIS pixels; b) the MODIS algorithm is designed to retrieve a distribution function of all possible LAI values of a pixel on the basis of the spectral information and biome type, taking the mean of the distribution function as the retrieved LAI (Knyazikhin et. al, 1998b; Tian et. al, 2000; Wang et. al, 2001). Theoretically it is possible that the LAI of a single MODIS pixel is not retrieved accurately, but the mean of multiple retrievals over a region with similar pixels is accurately retrieved. Therefore, averaging over a homogeneous area is required. The aggregated LAI map is then divided into several patches according to the similarity of LAI values (Figure 15). Each patch can be represented by the mean LAI value sufficiently well. Figure 17 shows the patch-by-patch relationship between the MODIS and aggregated LAI values. A much better agreement is achieved at the patch scale, as the comparisons in the case of 30 m resolution. However, only four points remain, hence R^2 and RMSE cannot be calculated due to the insufficient number of observations. Figure 18 shows the histograms of LAI values for the 10x10 km area obtained from aggregated LAI and the MODIS LAI fields. A t-test ($p=0.62$) indicates that the mean values of these histograms are not significantly different, thus suggesting satisfactory performance of the algorithm in this case study.

6 Discussion and Conclusions

It was found that pixel scale results are unreliable for a whole range of methods tested. Patch level comparisons improve the correlation between field measurements and satellite derived vegetation indices because this reduces the registration errors and the averaged field measurements are more representative of the mean LAI of the whole patch.

For a specific site, empirical approaches work well to produce a fine resolution LAI map from satellite data because the regression processes finds the best fit between field measurements

and satellite data and eliminates the problem of systematic bias. Various relationships such as linear (Fassnacht et. al., 1997; Peterson et. al., 1987; Chen and Cihlar, 1996; Chen et. al., 2002; Curran et. al., 1992; Running et. al., 1986; Nemani et. al., 1993), polynomial (Turner et. al., 1999), power (Peterson et. al., 1987), logarithm (Spanner et. al., 1994) and other (Gong et. al., 1995) regressions have been used to estimate LAI from TM images. Table 5 lists the regression models reported in literature that relate field LAI measurements and these vegetation indices derived from Landsat TM data for coniferous forests with R^2 values ranging from 0.32 to 0.97. These relationships are also influenced by the difference in LAI definition, field measurement method and atmospheric correction of the satellite image (Running et. al., 1986). Figure 19 plots these regression curves. One can see that the regression models are highly site-specific; there is no uniform relationship between vegetation indices and field measured LAI for all those sites, especially when the canopy is dense (high LAI) because the surface reflectance is insensitive to LAI change in this case. Therefore, although very good correlation between satellite derived vegetation indices and field measured LAI can be achieved for a specific site, empirical methods do not consider the physics behind the regression relationships and are highly site dependent, and thus cannot be generalized to very large areas or different sites, their utility is limited.

A patch-level comparison of the aggregated high resolution LAI map with corresponding MODIS LAI retrievals reveals good correspondence between the two and imbues confidence in the MODIS LAI and FPAR algorithm. However, we failed to adjust the LAI/FPAR algorithm to produce a fine resolution LAI map for this particular site. The ETM+ pixels coincide with the finest resolution that the algorithm can recognize and which is assumed to represent one biome type in each pixel. In the case of the Ruokolahti site, a forest biome can be mixed with understory sprigs, shrubs, mosses and grasses within the 30 m pixel, causing high uncertainties in the specification of biome type which is input to the algorithm. The creation of a finer than 30 m resolution Look-up-Table (LUT) is a possible solution to account for biome mixture at 30 m

resolution. Alternatively, radiative transfer models for multiple layer vegetation canopies which count in understory vegetation effect could be explored.

The single scattering albedo is a very important variable for LAI retrieval when using a radiative transfer based method. It depends on the size of the elementary volume and optical properties of scattering centers, although it is not clear as how to measure the mean single scattering albedo systematically over a site or how to account for the influence of understory vegetation and how it changes with scale. The single scattering albedo of an elementary volume could be retrieved using hyperspectral canopy reflectance and transmittance data (Wang et. al., 2002). An alternate way could be calculating from a shoot model according to the optical properties of a single needle.

This analysis also indicated that the reduced simple ratio (RSR), which includes red, near-infrared and shortwave infrared bands, is best correlated with field LAI measurements. Thus, it appears that the use of shortwave infrared band in MODIS LAI retrievals over needle leaf forests should be investigated.

Reference:

- Baret, F., Guyot, G., Begue, A., Maurel, P., and Podaire, A. (1988). Complementarity of middle infrared with visible and near-infrared reflectance of monitoring wheat canopies. *Remote Sens. Environ.*, 26:213-225.
- Beaulieu, J. M., and Goldberg, M. (1989), Hierarchy in picture segmentation: a stepwise optimization approach. *IEEE Trans. Pattern Anal. Mach. Intell.*, 11:150-163.
- Bonan, G. B. (1996), A Land Surface Model (LSM version 1.0) for ecological, hydrological, and atmospheric studies: *Technical Description and user's guide*, NCAR/TN-417+STR, 88-102.

- Brown, L., Chen, J. M., Leblanc, S. G., and Cihlar, J. (2000). A shortwave infrared modification to the simple ratio for LAI retrieval in Boreal forests: an image and model analysis. *Remote Sens. Environ.* 71:16-25.
- Butera, C. (1986). A correlation and regression analysis of percent canopy closure and TM spectral response for selected forest sites in San Juan national forest, Colorado. *IEEE Trans. Geosci. Remote Sens.*, 24:122-129.
- Chen, J. M. and Black, T. A. (1992). Defining leaf area index for non-flat leaves, *Plant, Cell and Environment*, 15:421-429.
- Chen, J. M., and Cihlar, J. (1996). Retrieving leaf area index of boreal conifer forests using Landsat TM images. *Remote Sens. Environ.*, 55:153-162.
- Chen, J. M., Pavlic, G., Brown, L., Cihlar, J., Leblanc, S. G., White, H. P., Hall, R. J., Peddle, D. R., King, D. J., Trofymow, J. A., Swift, E., Van der Sanden, J., and Pellikka, P. K. E. (2002). Derivation and validation of Canada-wide coarse-resolution leaf area index maps using high-resolution satellite imagery and ground measurements. *Remote Sens. Environ.*, 80:165-184.
- Collins, J. B., and Woodcock, C. E. (2000), Combining geostatistical methods and hierarchical scene models for analysis of multiscale variation in spatial data. *Geogr. Anal.*, 32(1):50-63.
- Curran, P. J., Dungan, J. L. and Gholz, H. L. (1992), Seasonal LAI in slash pine estimated with Landsat TM, *Remote Sens. Environ.*, 39:3-13.
- Dickinson, R. E., Henderson-sellers, A., Kennedy, P. J., and Wilson, M. F. (1986), Biosphere-atmosphere transfer scheme (BATS) for the NCAR Community Climate Model, *Tech. Note TN-275+STR*, National Center for Atmospheric Research, Colorado, pp. 72.

- Fassnacht, K. S., Gower, S. T., MacKenzie, M. D., Nordheim, E. V., and Lillesand, T. M. (1997). Estimating the leaf area index of north central Wisconsin forest using the Landsat Thematic Mapper. *Remote Sens. Environ.*, 61:229-245.
- Foley, J. A., Levis, S., Prentice, I. C., Pollard, D. and Thompson, S. L. (1998), Coupling dynamic models of climate and vegetation, *Global Change Biol.*, 4:561-579.
- Franklin, J. (1986). Thematic mapper analysis of coniferous forest structure and composition. *Int. J. Remote Sens.*, 10:1287-1301.
- Gong, P., Pu, R. and Miller, J. R. (1995) Coniferous forest leaf area index estimation along the Oregon Transect using Compact Airborne Spectrographic Imager data, *PE&RS*, 61:1107-1117.
- Häme, T., Stenberg, P., Andersson, K., Rauste, Y., Kennedy, P., Folving, S. and Sarkeala, J. (2001), AVHRR-based forest proportion map of the Pan-European area. *Remote Sens. Environ.* 77: 76-91.
- Kimes, D., Knyazikhin, Y., Privette, J., Abuelgasim, A., and Gao, F. (2000), Inversion methods for physically-based models. *Remote Sens. Rev.*, 18: 381-439.
- Knyazikhin, Y., Martonchik, J. V., Myneni, R. B., Diner, D. J., and Runing, S. (1998a), Synergistic algorithm for estimating vegetation canopy leaf area index and fraction of absorbed photosynthetically active radiation from MODIS and MISR data. *J. Geophys. Res.*, 103:32,257-32,275.
- Knyazikhin, Y., Martonchik, J. V., Diner, D. J., Myneni, R. B., Verstraete, M., Pinty, B. and Gorbon, N. (1998b), Estimation of vegetation canopy leaf area index and fraction of absorbed photosynthetically active radiation from atmosphere-corrected MISR data. *J. Geophys. Res.*, 103:32,239-32,256.

- Knyazikhin, Y., Mieben, G., Panfyorov, O. and Gravenhorst, G. (1997), Small-scale study of three dimensional distribution of photosynthetically active radiation in forest, *Agric. For. Meteorol.*, 88:215-239.
- Li-COR, inc. (1992), *LAI-2000 plant canopy analyzer instruction manual*. pp.4-12.
- MacDonald, R. B., and Hall, F. G. (1980), Global crop forecasting. *Science* 208:670-679.
- Markham, B. L., and Townshend, J. R. G. (1981), Landcover classification accuracy as a function of sensor spatial resolution. In *proceedings of the 15th international symposium on Remote Sensing of Environment held in Ann Arbor, Michigan, U. S. A.* pp.1,075-1,090.
- Miller, J. B. (1967), A formula for average foliage density, *Aust. J. Bot.*, 15:141-144.
- Myneni, R. B., Hoffman, S., Knyazikhin, Y., Privette, J. L., Glassy, J., Tian, Y., Wang, Y., Song, X., Zhang, Y., Smith, G. R., Lotsch, A., Friedl, M., Morisette, J. T., Votava, P., Nemani, R. R. and Running, S. W. (2002). Global products of vegetation leaf area and fraction absorbed PAR from year one of MODIS data. *Remote Sens. Environ.*, 83: 214-231
- Myneni, R. B., Nemani, R. R., and Running, S. W. (1997), Estimation of global leaf area index and absorbed PAR using radiative transfer models. *IEEE Trans. Geosci. Remote Sens.*, 35:1380-1393.
- Myneni, R. B., Knyazikhin, Y., Zhang, Y., Tian, Y., Wang, Y., Lotsch, A., Privette, J. L., Morisette, J. T., Running, S. W., Nemani, R., Glassy, J., Votava, P., (1999), MODIS leaf area index (LAI) and fraction of photosynthetically active radiation absorbed by vegetation (FPAR) product (MOD15) algorithm theoretical basis document, Version 4.0, pp. 5.

- Nemani, R., Pierce, L., Running, S., and Band, L. (1993). Forest ecosystem process at the watershed scale: sensitivity to remotely-sensed leaf area index estimates. *Int. J. Remote Sens.*, 14:2519-2534.
- Peterson, D. L., Spanner, M. A., Running, R. W. and Band, L. (1987), Relationship of thematic mapper simulator data to leaf area index of temperate coniferous forest. *Remote Sens. Environ.*, 22:323-341.
- Privette, J. L., Myneni, R. B., Knyazikhin, Y., Mukufute, M., Roberts, G., Tian, Y., Wang, Y., and Leblanc, S. G. (2002), Early spatical and temporal validation of MODIS LAI product in Africa. *Remote Sens. Environ.*, 83: 232-243.
- Rahman, H., and Didieu, G. (1994), SMAC: a simplified method for the atmospheric correction of satellite measurements in the solar spectrum. *Int. J. Remote Sens.* 15:123-143.
- Running, S. W., Peterson, D. L., Spanner, M.A. and Teuber, K. B. (1986), Remote sensing of coniferous forest leaf are, *Ecology*, 67:273-276.
- Sellers, P. J., Randall D. A., Betts A. K., Hall F. G., Berry J. A., Collatz G. J., Denning A. S., Mooney H. A., Nobre C. A., Sato N., Field C. B., Henderson-sellers A.. (1997), Modeling the exchanges of energy, water, and carbon between continents and the atmosphere. *Science*, 275:502-509.
- Spanner, M., Johnson, L., Miller, J., McCreight, R., Freemantle, J. and Gong, P. (1994). Remote sensing of seasonal leaf area index across the Oregon Transect, *Ecol. Appl.*, 4:258-271.
- Spanner, M. A., Pierce, L. L., Peterson, D. L, and Running, S. W. (1990), Remote sensing of temperate coniferous forest leaf area index. The influence of canopy closure, understory vegetation and background reflectance. *Int. J. Remote Sens.*, 11:95-111.

- Stenberg, P. (1996). Correcting LAI-2000 estimates for the clumping of needles in shoots of conifers. *Agricultural and Forest Meteorology*, 79:1-8.
- Tian, Y., Woodcock, C. E., Wang, Y., Privette, J. L., Shabanov, N. V., Zhou, L., Buermann, W., Dong, J., Veikkanen, B., Hame, T., Ozdogan M., Knyazikhin Y., and Myneni, R. B., (2002a), Multiscale Analysis and Validation of the MODIS LAI Product over Maun, Botswana, I. uncertainty assessment, *Remote Sens. Environ.* 83:414-430.
- Tian, Y., Woodcock, C. E., Wang, Y., Privette, J. L., Shabanov, N. V., Zhou, L., Buermann, W., Dong, J., Veikkanen, B., Hame, T., Ozdogan M., Knyazikhin Y., and Myneni, R. B., (2002b), Multiscale Analysis and Validation of the MODIS LAI Product over Maun, Botswana, II. Sampling strategy, *Remote Sens. Environ.* 83:431-441.
- Tian, Y., Wang, Y., Zhang, Y., Knyazikhin, Y., Bogaert, J., and Myneni, R. B. (2002c), Radiative Transfer Based Scaling of LAI/FPAR Retrievals From Reflectance Data of Different Resolutions, *Remote Sens. Environ.*, 84:143-159.
- Turner, D. P., Cohen, W. B., Kennedy, R. E., Fassnacht, K. S. and Briggs, J.M. (1999). Relationships between leaf area index and Landsat TM spectral vegetation indices across three temperate zone sites, *Remote Sens. Environ.*, 70:52-68.
- Wang, Y., Tian, Y., Zhang, Y., El-Saleous, N., Knyazikhin, Y., Vermote, E. and Myneni, R. B. (2001), Investigation of product accuracy as a function of input and model uncertainties: Case study with SeaWiFS and MODIS LAI/FPAR algorithm, *Remote Sens. Environ.*, 78:296-311.
- Woodcock, C. E., Collins, J. B., and Jupp, D. L. B. (1997), Scaling remote sensing models. In *Scaling-up from Cell to Landscape* (P. R. Van Gardingen, G. M. Foody and P. J. Curran, Eds.), Cambridge, United Kingdom, pp. 61-77.

Woodcock, C. E., and Harward, V. J. (1992), Nested-hierarchical scene models and image segmentation. *Int. J. Remote Sens.* 13(16):3,167-3,187.

Table Captions

Table 1. Means and standard deviations of ETM+ reflectances over the dense, intermediate and young forests.

Table 2. Mean, standard deviation and t-test results of LAI for 50 m and 25 m grid locations in the dense, young and intermediate forests.

Table 3. Mean ETM+ reflectances over patches, their standard deviations and number of pixels per segment.

Table 4. Mean Leaf Area Index (LAI) of segments, standard deviations, coefficients of variation, and number of samples in the segment.

Table 5. Regression models reported in literature to relate Leaf Area Index (LAI) and vegetation indices derived from Landsat TM data .

Figure Captions

Figure 1. Ruokolahti field campaign sampling strategy.

Figure 2. Histograms of atmospherically corrected ETM+ reflectances at (a) red and (b) NIR spectral bands.

Figure 3. Histograms of effective LAI values for young, intermediate and dense forests, at resolutions of 25m and 50 m.

Figure 4. Correlation between LAI measured at 50 m grid and corresponding 25 m subgrid.

Figure 5. (a) Contour plot of LAI values for the validation site and (b) its high resolution CCD image.

Figure 6. Correlation between LAI retrieved by the MODIS LAI algorithm at 30 m resolution and field measured LAI at the pixel scale. (a) Before LUT adjustment; (b) After LUT adjustment.

Figure 7. The schemes of comparison between satellite pixels and field samples. (a) pixel-by-pixel comparison; (b) patch-by-patch comparison. Circles represent field samples and squares represent satellite pixels.

Figure 8. (a) RGB image of the 1 km region of Ruokolahti from ETM+ band 4, 3, 2 (b) Map of the 1 km region using a segmentation procedure.

Figure 9. Correlation between LAI retrieved by the MODIS LAI and FPAR algorithm at 30 m resolution and field measured LAI at patch scale: (a) before LUT adjustment; (b) after LUT adjustment.

Figure 10. Correlation between the normalized differential vegetation index (NDVI) and field measured LAI at (a) pixel comparison and (b) patch scale.

Figure 11. Correlation between simple ratio (SR) and field-measured LAI at (a) pixel and (b) patch scale.

Figure 12. Patch level comparison between Leaf Area Index (LAI) and reduced simple ratio (RSR).

Figure 13. (a) 10x10 km LAI maps derived from the ETM+ image using the relationship (4) and (b) its 1x1 km central part.

Figure 14. MODIS pixels in the 10x10 km area. Green: LAI value produced by the main algorithm; Red: LAI is produced by the backup algorithm; Blue: cloud contaminated pixel; Black: water or barren.

Figure 15. Contour plot of Leaf Area Index (LAI) aggregated from the fine resolution ETM+ LAI map.

Figure 16. Pixel-by-pixel correlation between the MODIS and aggregated Leaf Area Index (LAI) values.

Figure 17. Patch level correlation between the MODIS and aggregated Leaf Area Index (LAI) values.

Figure 18. Histograms of LAI values for the 10x10 km area obtained from aggregated ETM+ LAI and the MODIS LAI fields.

Figure 19. Regression curves between simple ratio (SR) and LAI reported in literature.

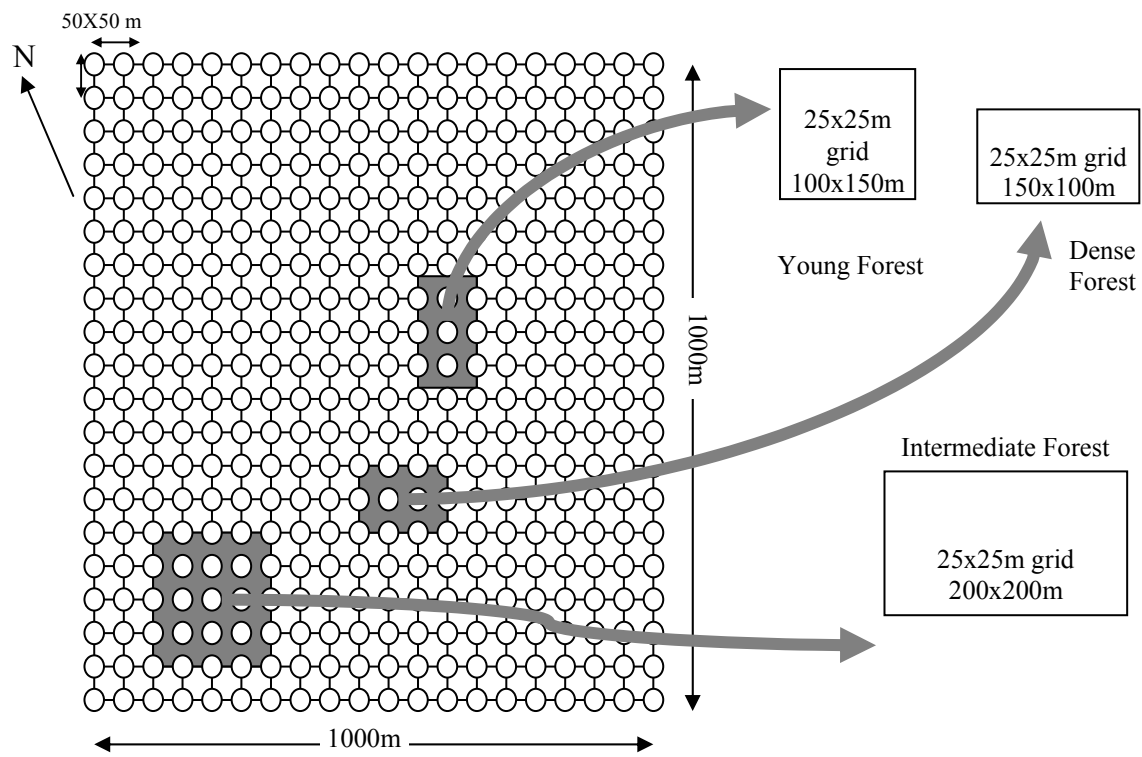
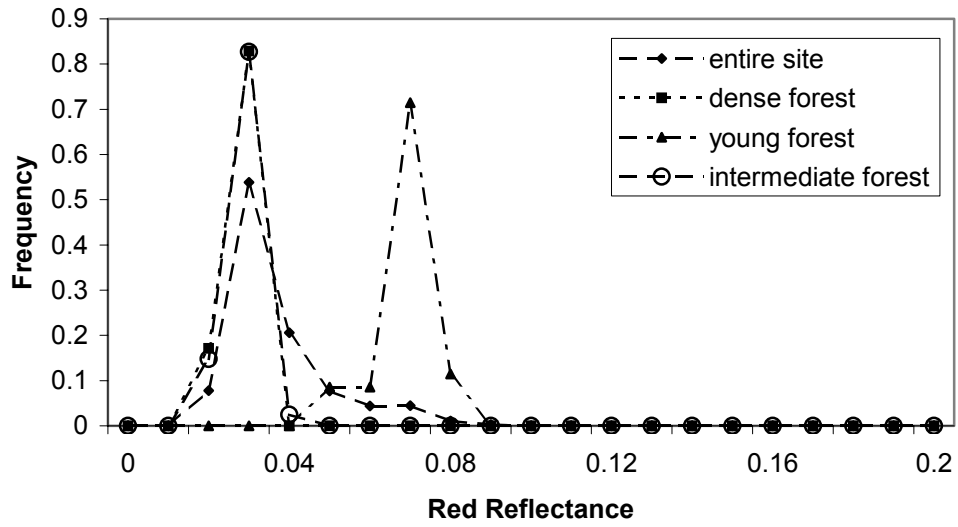


Figure 1. Ruokolahti field campaign sampling strategy.

(a)



(b)

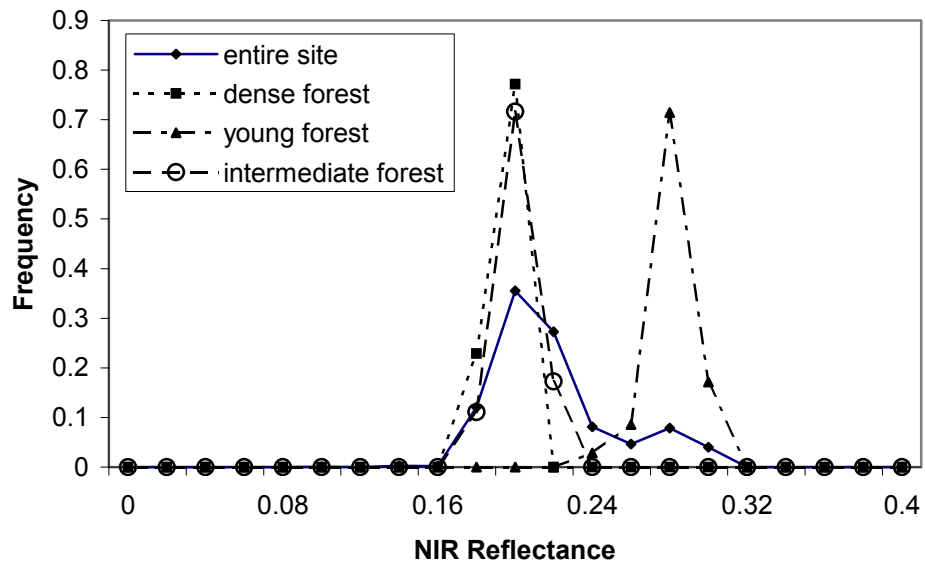


Figure 2. Histograms of atmospherically corrected ETM+ reflectances at (a) red and (b) NIR spectral bands.

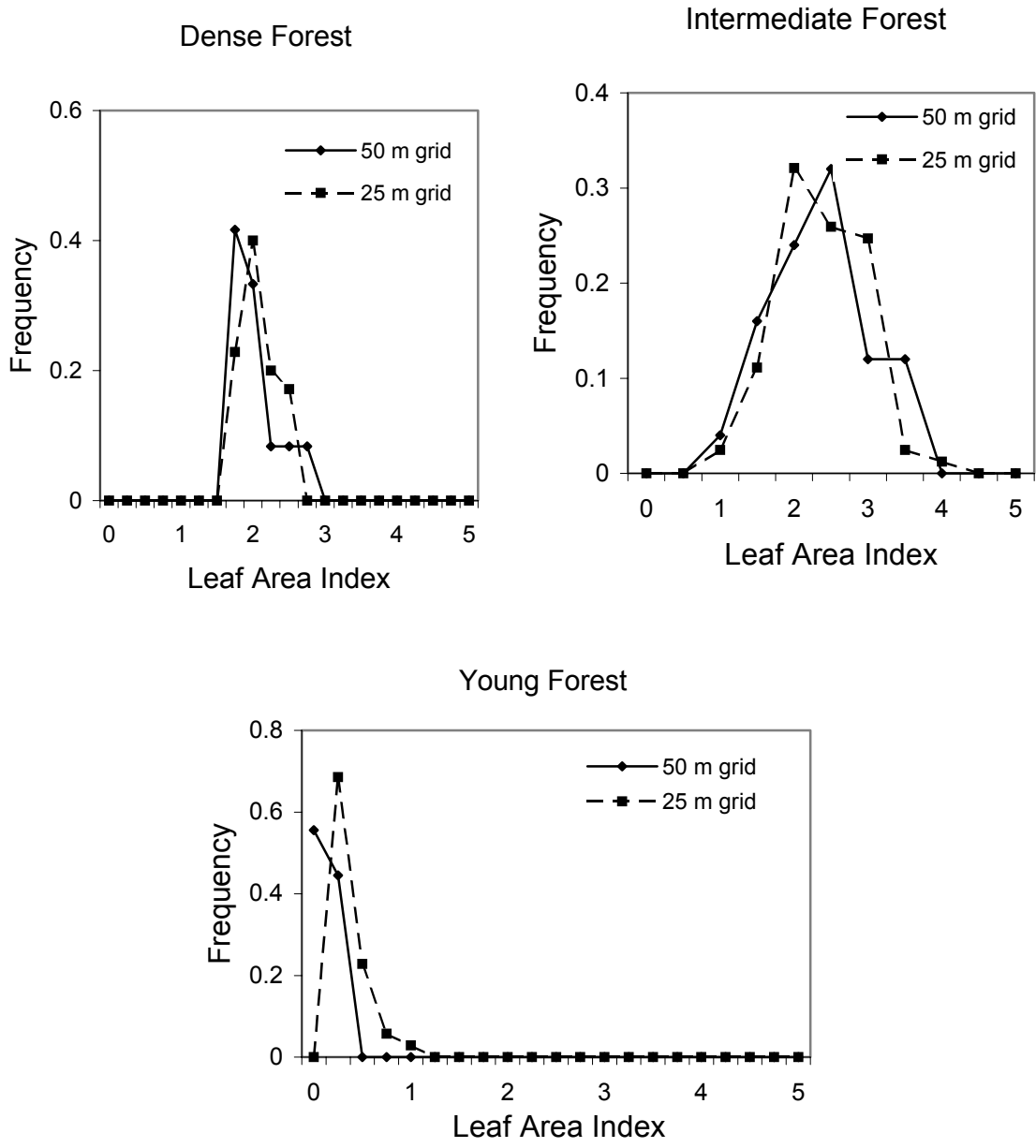


Figure 3. Histograms of effective LAI values for young, intermediate and dense forests, at resolutions of 25m and 50 m.

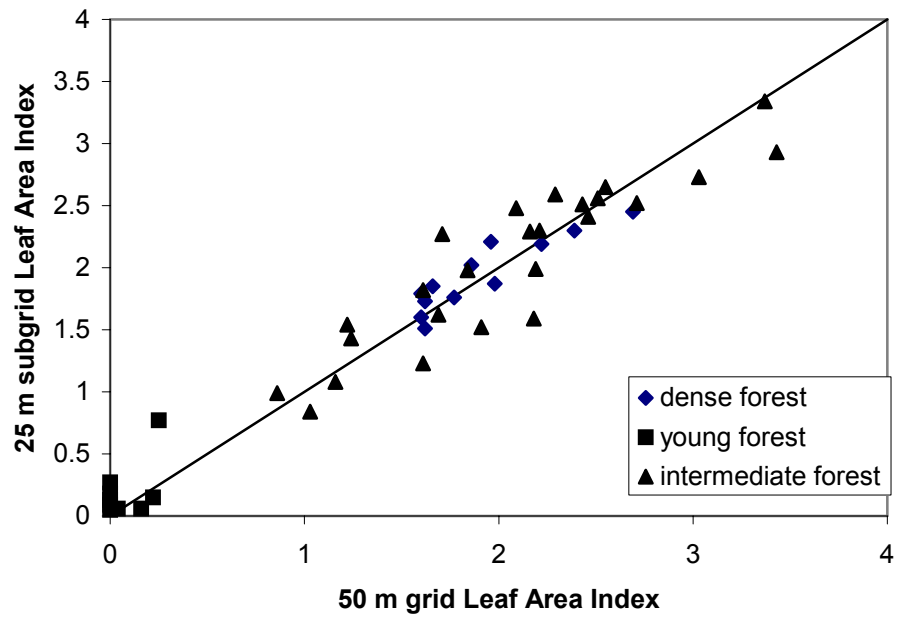
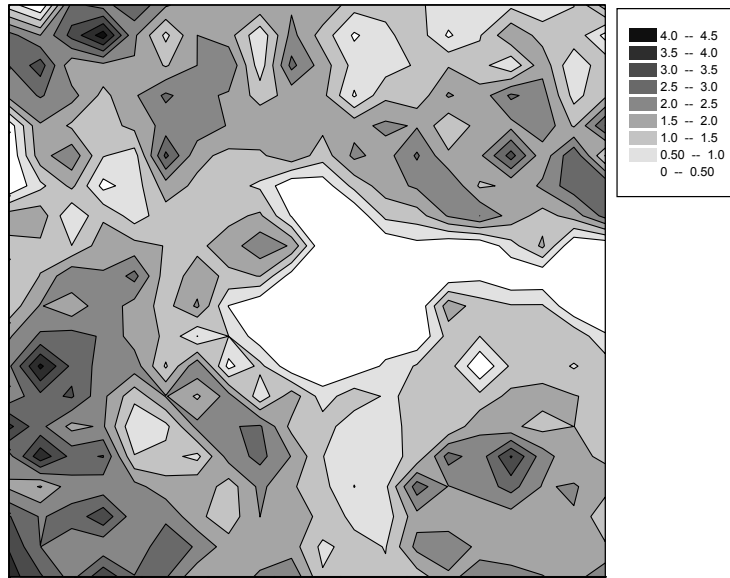


Figure 4. Correlation between LAI measured at 50 m grid and corresponding 25 m subgrid.

(a)

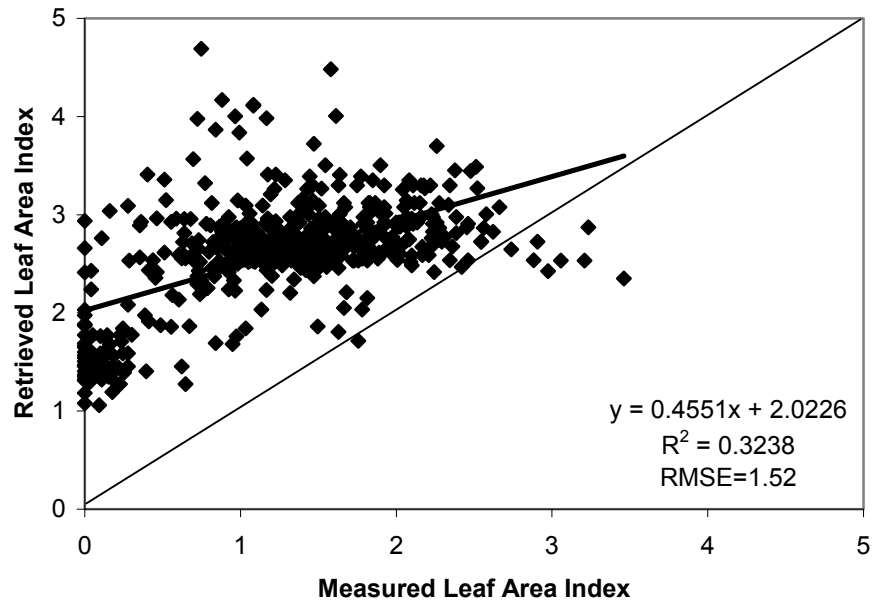


(b)



Figure 5. (a) Contour plot of LAI values for the validation site and (b) its high resolution CCD image.

(a)



(b)

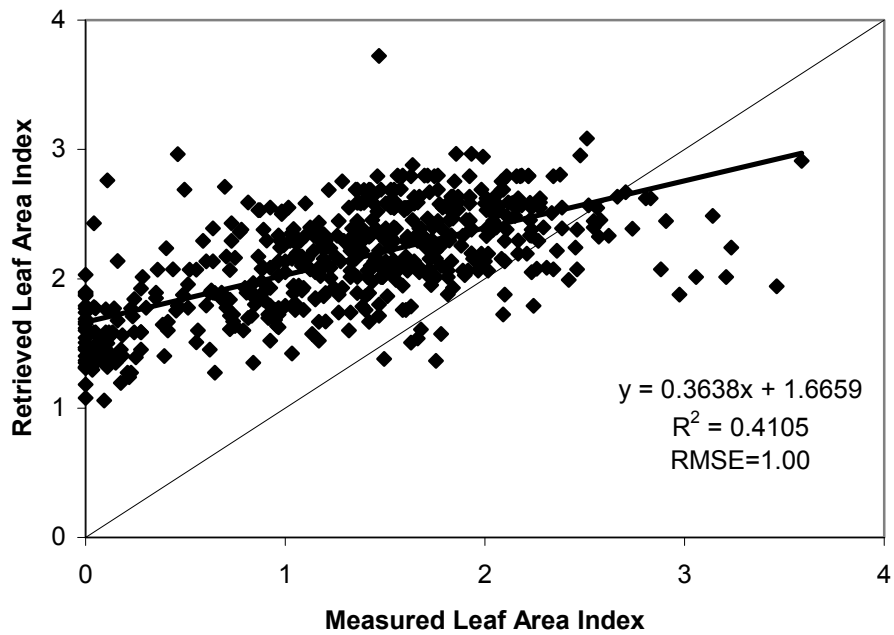
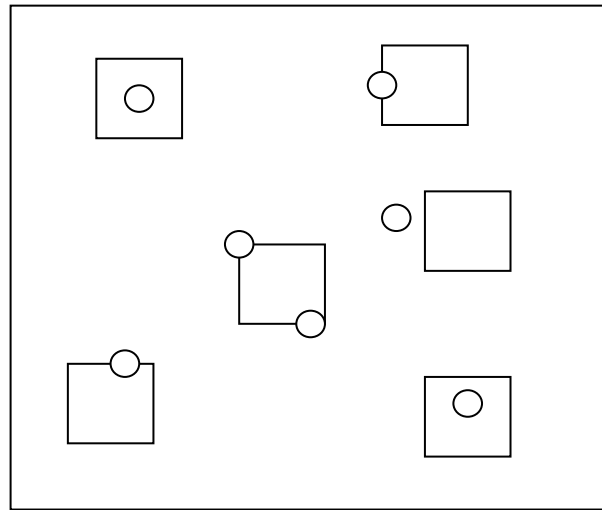


Figure 6. Correlation between LAI retrieved by the MODIS LAI algorithm at 30 m resolution and field measured LAI at the pixel scale. (a) Before LUT adjustment; (b) After LUT adjustment.

(a)



(b)

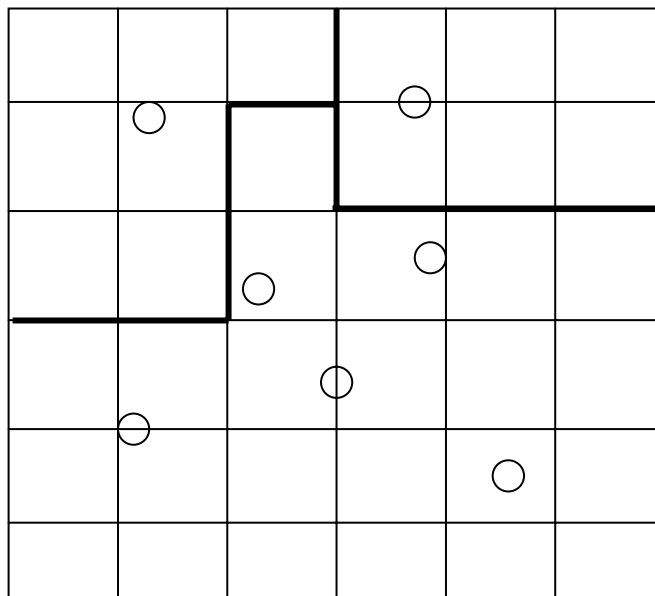


Figure 7. The schemes of comparison between satellite pixels and field samples. (a) pixel-by-pixel comparison; (b) patch-by-patch comparison. Circles represent field samples and squares represent satellite pixels.

(a)



(b)

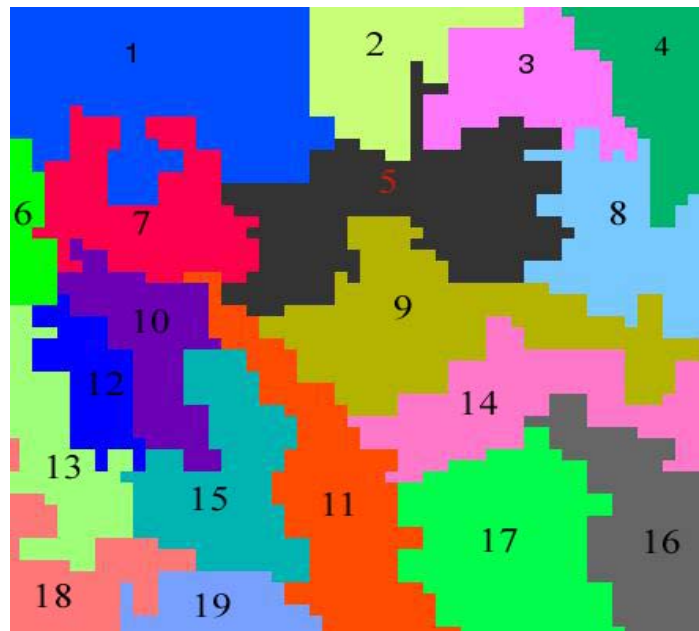
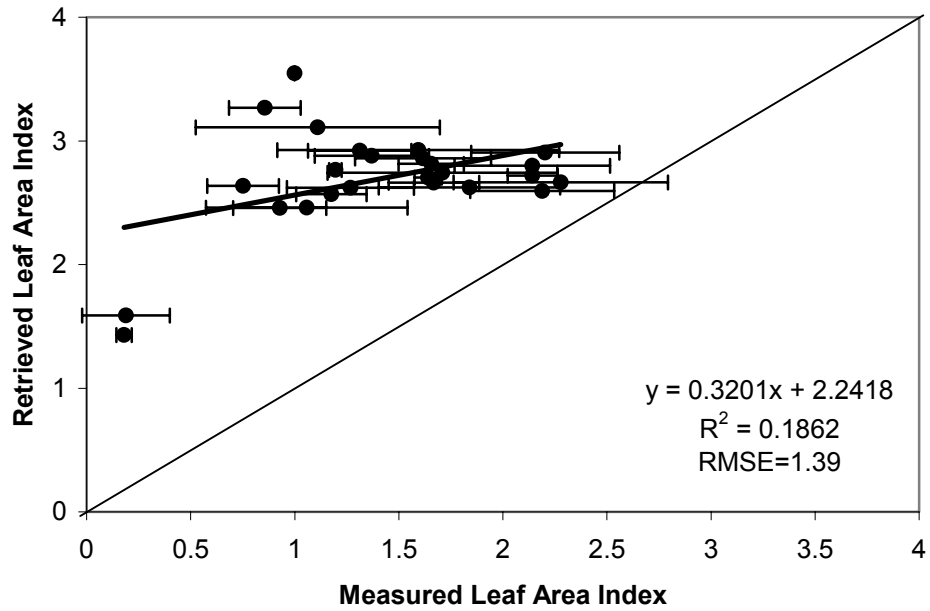


Figure 8. (a) RGB image of the 1 km region of Ruokolahti from ETM+ band 4, 3, 2 (b) Map of the 1 km region using a segmentation procedure.

(a)



(b)

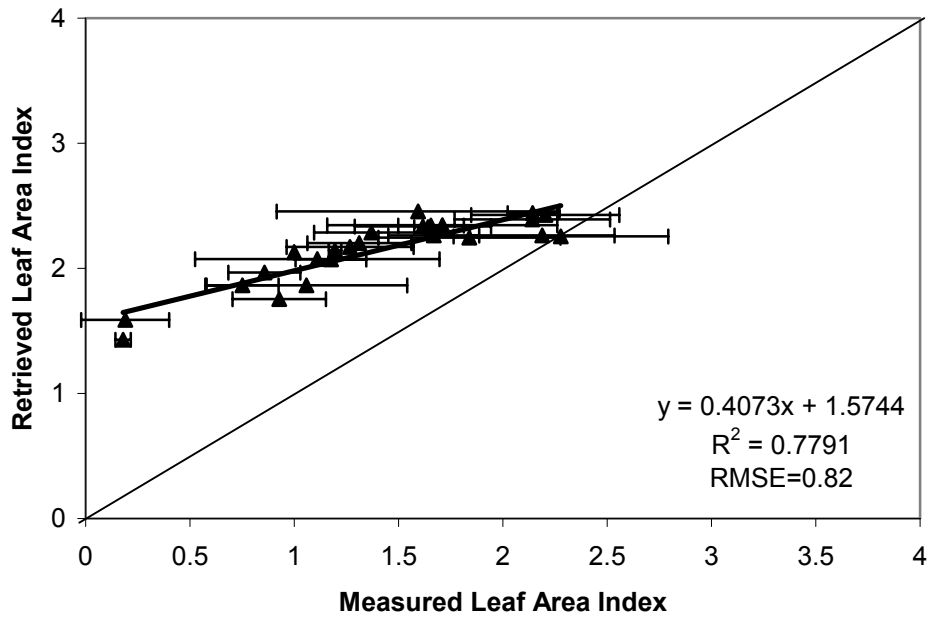
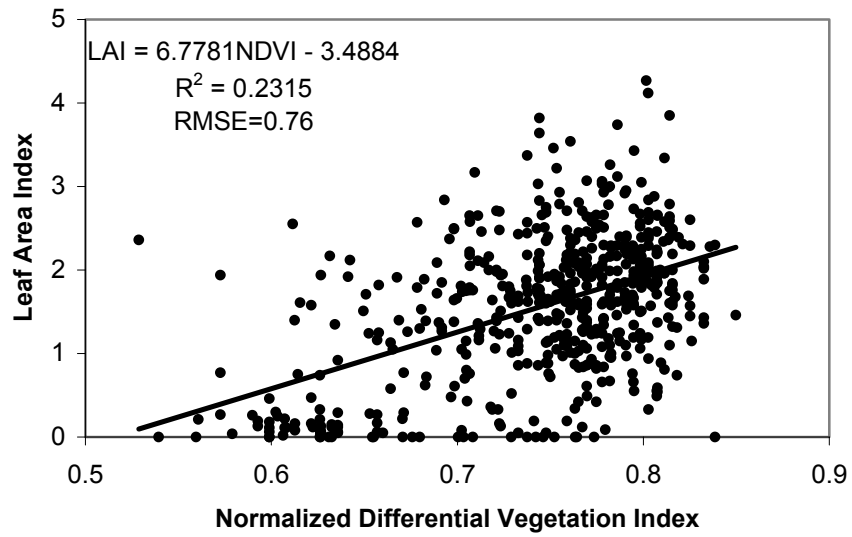


Figure 9. Correlation between LAI retrieved by the MODIS LAI and FPAR algorithm at 30 m resolution and field measured LAI at patch scale: (a) before LUT adjustment; (b) after LUT adjustment.

(a)



(b)

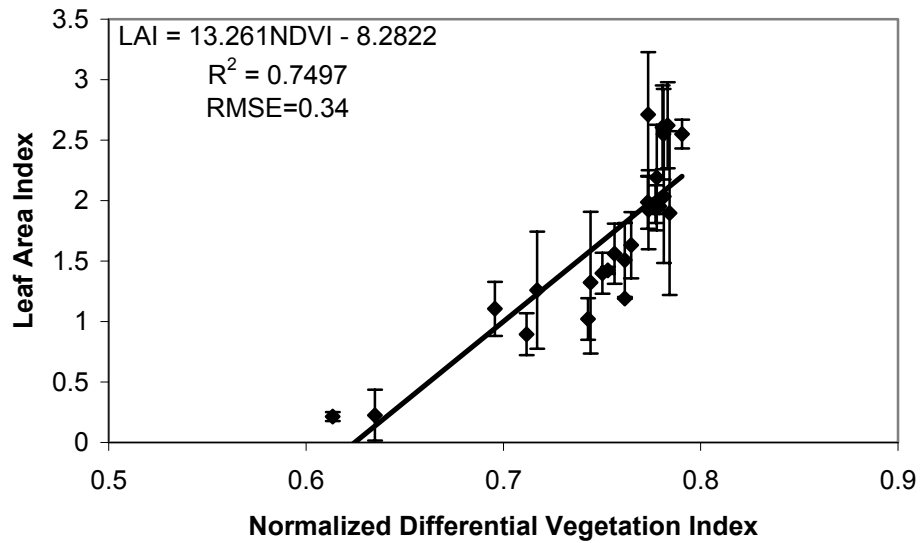
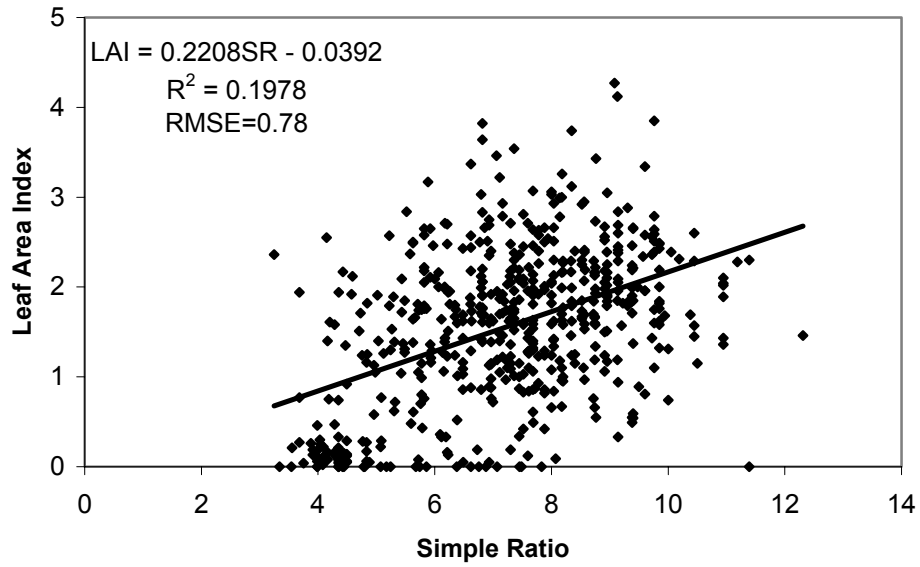


Figure 10. Correlation between the normalized differential vegetation index (NDVI) and field measured LAI at (a) pixel comparison and (b) patch scale.

(a)



(b)

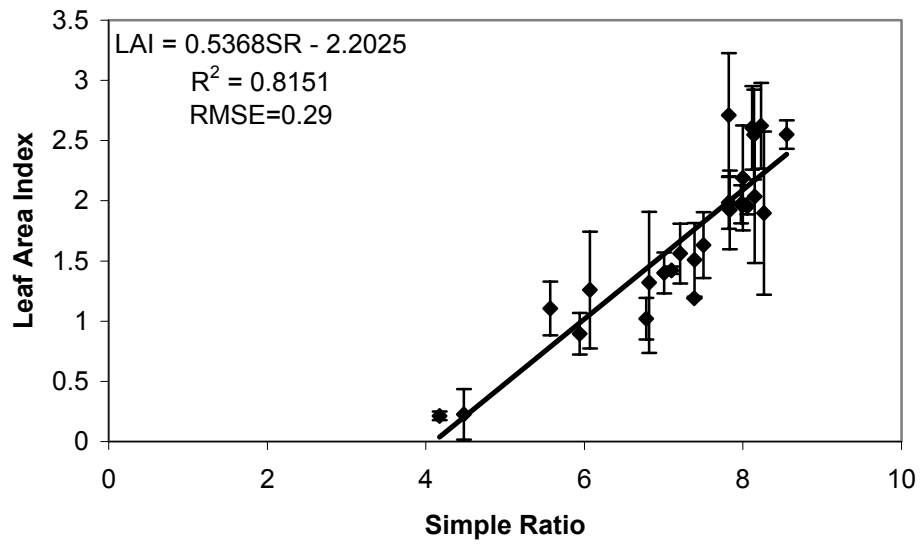


Figure 11. Correlation between simple ratio (SR) and field-measured LAI at (a) pixel and (b) patch scale.

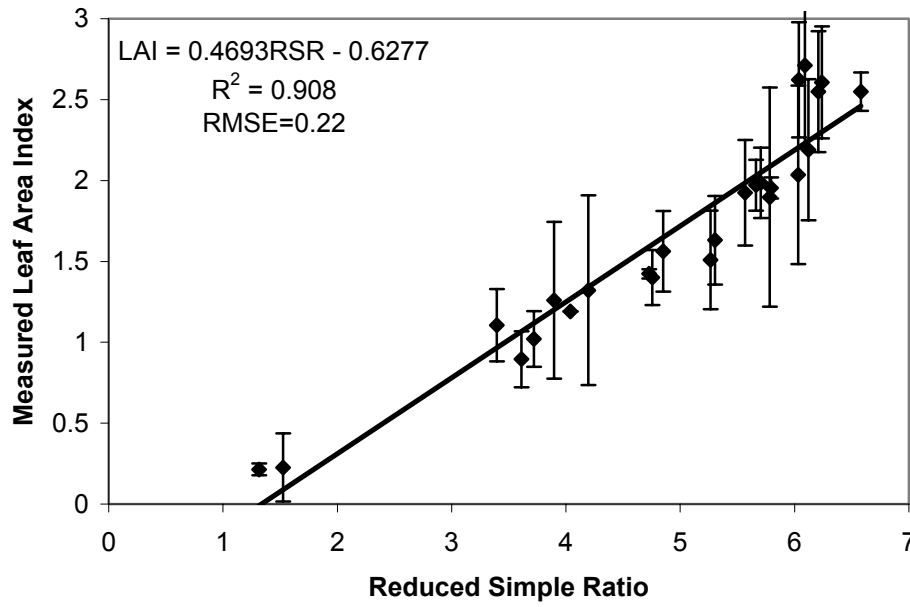
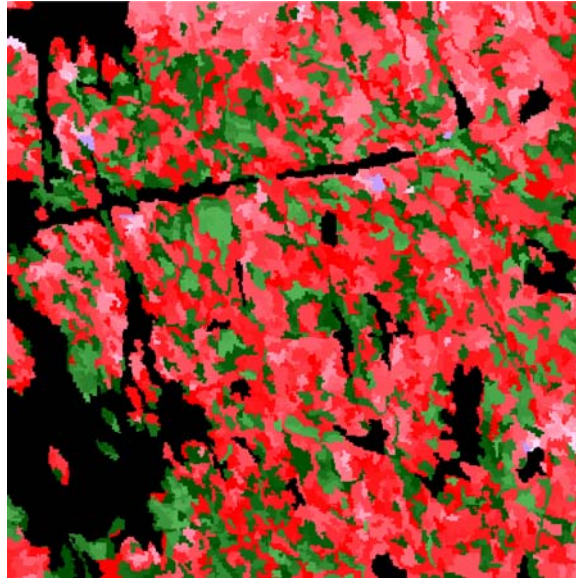


Figure 12. Patch level comparison between Leaf Area Index (LAI) and reduced simple ratio (RSR).

(a)



(b)

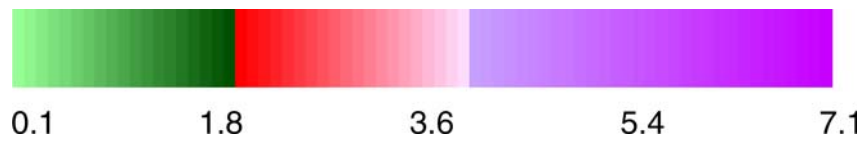
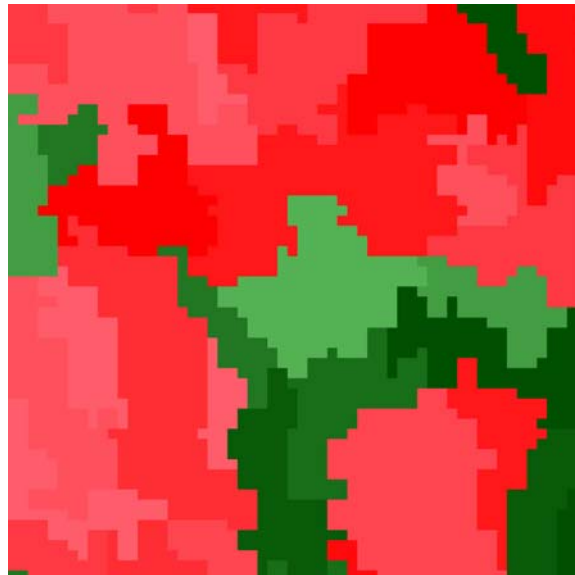


Figure 13. (a) 10x10 km LAI maps derived from the ETM+ image using the relationship (4) and (b) its 1x1 km central part.

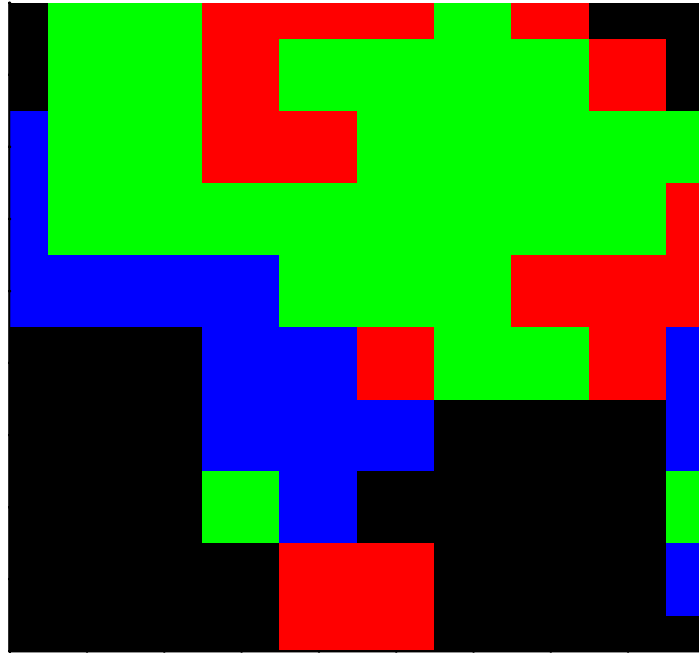


Figure 14. MODIS pixels in the 10x10 km area. Green: LAI value produced by the main algorithm; Red: LAI is produced by the backup algorithm; Blue: cloud contaminated pixel; Black: water or barren.

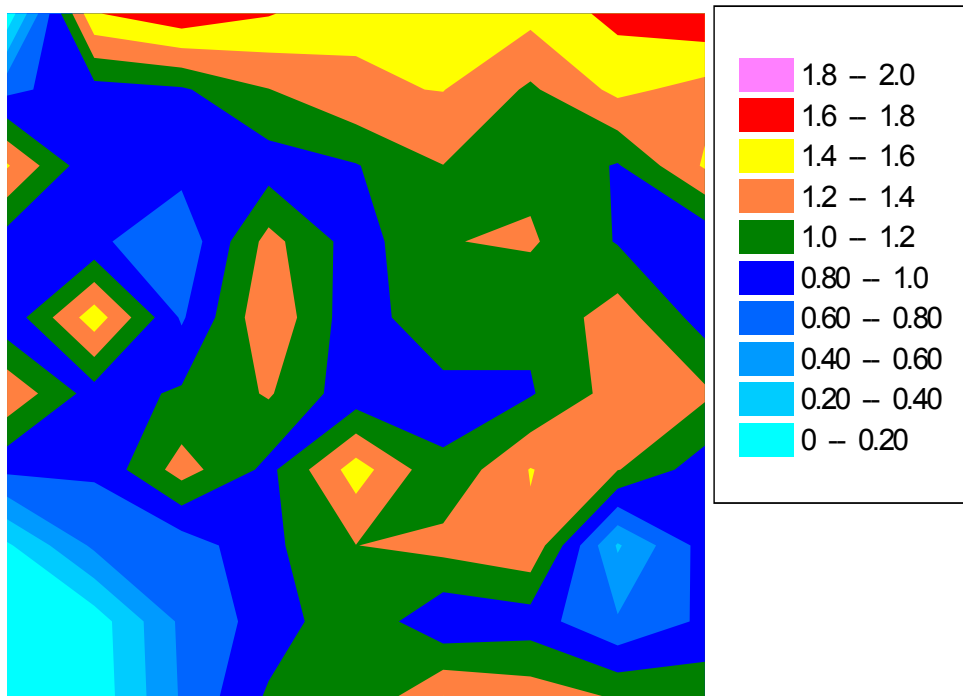


Figure 15. Contour plot of Leaf Area Index (LAI) aggregated from the fine resolution ETM+ LAI map.

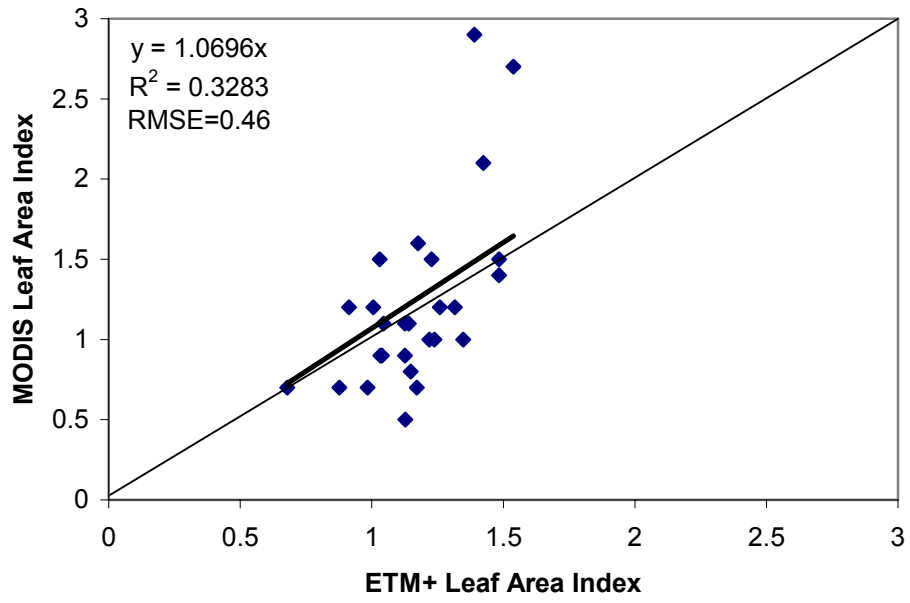


Figure 16. Pixel-by-pixel correlation between the MODIS and aggregated Leaf Area Index (LAI) values.

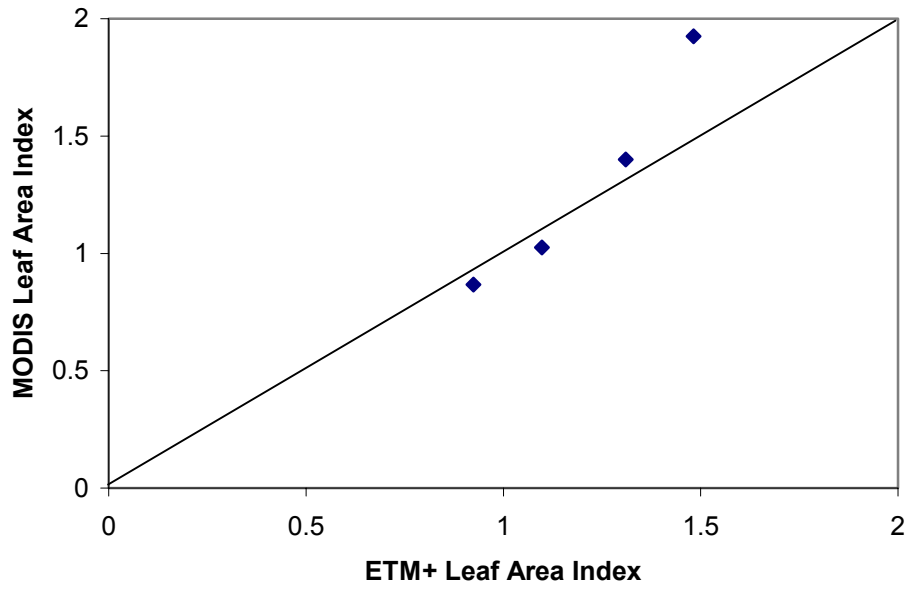


Figure 17. Patch level correlation between the MODIS and aggregated Leaf Area Index (LAI) values.

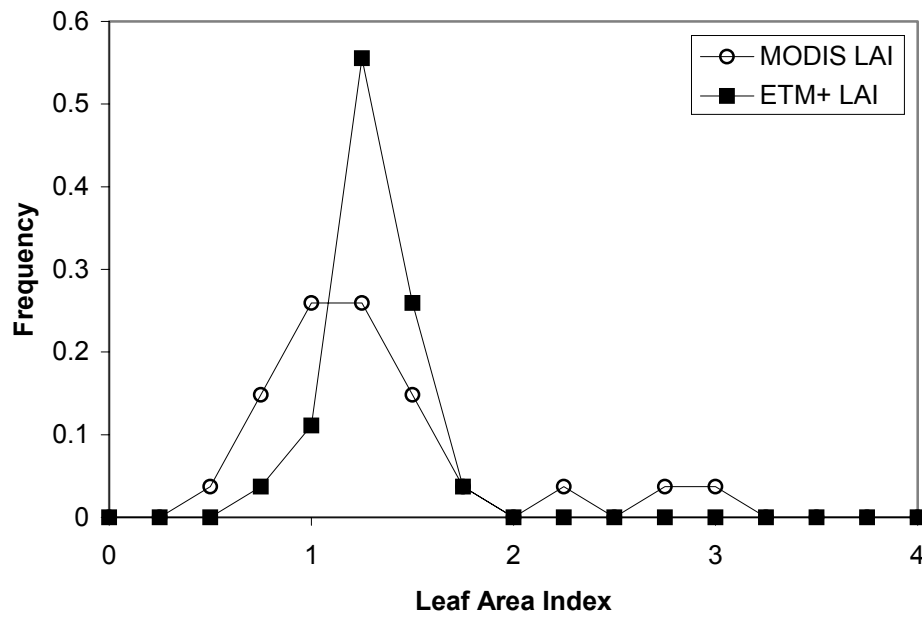


Figure 18. Histograms of LAI values for the 10x10 km area obtained from aggregated ETM+ LAI and the MODIS LAI fields.

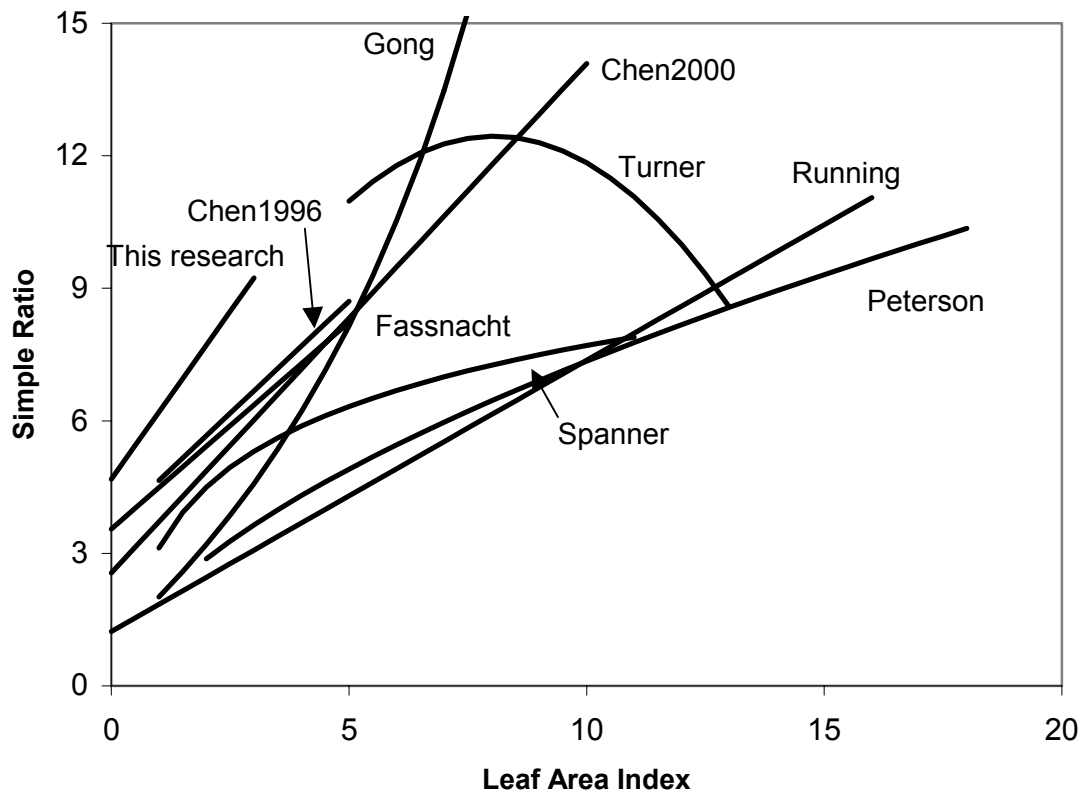


Figure 19. Regression curves between simple ratio (SR) and LAI reported in literature.

Table 1. Means and standard deviations of ETM+ reflectances over the dense, intermediate and young forests.

	Dense Forest	Intermediate Forest	Young Forest	Entire site
Mean red	0.023	0.025	0.065	0.032
STD red	0.004	0.003	0.007	0.012
Mean NIR	0.19	0.19	0.27	0.21
STD NIR	0.006	0.008	0.013	0.031

Table 2. Mean, standard deviation and t-test results of LAI for 50 m and 25 m grid locations in the dense, young and intermediate forests.

	Dense Forest	Intermediate Forest	Young Forest
Mean (50m)	1.91	2.06	0.07
STD (50m)	0.36	0.68	0.11
Mean (25m)	1.95	2.10	0.22
STD (25m)	0.26	0.56	0.19
t-test (P value)	0.68	0.76	0.04

Table 3. Mean ETM+ reflectances over patches, their standard deviations and number of pixels per segment.

Patch No.	Red band		NIR band		Number of pixels
	Mean	STD	Mean	STD	
1	0.02311	1.21E-05	0.1883	0.0003	218
2	0.02685	3.25E-05	0.2014	0.000172	67
3	0.03778	2.98E-05	0.2561	0.000235	79
4	0.03489	3.60E-05	0.2378	0.00032	38
5	0.02895	2.96E-05	0.2087	0.00036	286
7	0.03185	6.05E-05	0.1933	0.000362	149
8	0.02445	3.66E-05	0.2021	0.000359	121
9	0.06119	9.27E-05	0.274	0.000253	244
10	0.02503	1.78E-05	0.1849	8.31E-05	121
11	0.03958	65E-05	0.2205	0.000373	175
12	0.02176	5.18E-06	0.1766	6.05E-05	74
13	0.0242	1.04E-05	0.1991	5.56E-05	91
14	0.03611	3.30E-05	0.2145	0.0002	149
15	0.02527	1.07E-05	0.1979	7.81E-05	174
16	0.02773	1.33E-05	0.1968	65E-05	44
17	0.02366	1.16E-05	0.185	6.07E-05	202
18	0.02365	1.22E-05	0.185	5.41E-05	26

Table 4. Mean Leaf Area Index (LAI) of segments, standard deviations, coefficients of variation, and number of samples in the segment.

Patch No.	Mean LAI	STD	STD/Mean	Number of samples
1	2.035	0.5514	0.270958	42
2	1.631	0.2743	0.168179	14
3	1.02	0.1721	0.168725	16
4	1.322	0.586	0.443268	10
5	1.562	0.2486	0.159155	43
7	1.259	0.4844	0.38475	26
8	1.897	0.6777	0.357248	22
9	0.2258	0.2106	0.932684	38
10	1.509	0.3049	0.202054	16
11	1.105	0.2236	0.202353	30
12	2.606	0.3465	0.132962	13
13	2.623	0.3557	0.135608	17
14	0.895	0.1727	0.192961	28
15	1.924	0.327	0.169958	31
16	1.423	0.02948	0.020717	10
17	1.986	0.2177	0.109617	34
18	2.712	0.5147	0.189786	8

Table 5. Regression models reported in literature to relate Leaf Area Index (LAI) and vegetation indices derived from Landsat TM data .

Vegetation Index	Field LAI measurements	Equation	R ²	Author
NDVI/SR	Allometric method	LAI=0.5724+0.0989LAI-0.0114LAI ² +0.0004LAI ³	0.74	Turner et. al. (1999)
		SR=2.2282+2.5376LAI-0.1576LAI ²	0.59	
NDVI/SR	Allometric method	NDVI= 0.0377LAI+0.607	0.72	Fassnacht et. al. (1997)
		SR= 0.9357LAI+3.552	0.71	
SR	Allometric method	SR=1.92LAI ^{0.583}	0.91	Peterson et. al. (1987)
		SR=1.92+0.532LAI	0.83	
NDVI/SR	LAI-2000 and TRAC*	NDVI=0.032LAI+0.635	0.42	Chen and Cihlar, (1996)
		SR=1.014LAI+3.637	0.49	
SR	LAI-2000 and TRAC*	SR=1.153LAI+2.56	0.66	Chen et. al. (2002)
SR	Ceptometer	SR=3.1196+5857log(LAI)	0.97	Spanner et. al., (1994)
NDVI/SR	LAI-2000	NDVI=1.2383/(1/LAI+0.9061)-0.3348	0.87	Gong et. al. (1995).
		SR=0.96/(1/LAI-0.066)+0.987	0.88	
NDVI	Allometric method	LAI=33.99NDVI-121	0.75	Curran et. al. (1992)
SR	Allometric method	SR=0.614LAI+1.23	0.82	Running et. al. (1986)
NDVI	Allometric method	NDVI=0.03LAI+0.6	0.32	Nemani et. al. (1993)